Computers in Biology and Medicine 40 (2010) 643–649

Contents lists available at ScienceDirect

Computers in Biology and Medicine

journal homepage: www.elsevier.com/locate/cbm

Analysis of unpredictable components within QRS complex using a finite-impulse-response prediction model for the diagnosis of patients with ventricular tachycardia

Chun-Cheng Lin *

Department of Electrical Engineering, National Chin-Yi University of Technology, Taichung, Taiwan

ARTICLE INFO

Article history:
Received 27 July 2009
Accepted 12 May 2010

Keywords:
Signal-averaged electrocardiogram
Ventricular late potentials
Unpredictable intra-QRS potentials
Ventricular tachycardia
Finite-impulse-response prediction model

ABSTRACT

This study proposes a finite-impulse-response (FIR) prediction model to analyze the unpredictable intra-QRS potentials (UIQP) for identifying ventricular tachycardia patients with high-risk ventricular arrhythmias. The simulation study shows that a QRS complex including abnormal intra-QRS potentials (AIQP) has a higher UIQP and UIQP-to-QRS ratio in comparison with one without AIQP. The clinical results demonstrate that the mean UIQP-to-QRS ratios of VT patients in leads *X*, *Y* and *Z* were significantly larger than those of the normal subjects, and the linear and logical combination of UIQP-to-QRS ratios and ventricular late potential parameters can enhance diagnosis performance for VT patients.

1. Introduction

In recent years, the signal-averaged electrocardiogram (SAECG) has become an important non-invasive tool for the risk stratification of ventricular arrhythmias to prevent sudden cardiac death [1–4]. Time-domain ventricular late potentials (VLP) analysis has established the clinical value for stratifying the risk of development of sustained ventricular arrhythmias in patients recovering from myocardial infarction, and for the identification of patients with ischemic heart disease and unexplained syncope [4]. Recently, the VLP parameters have also been applied to assess the risk of ventricular arrhythmias for symptomatic and asymptomatic patients with Brugada syndrome [5], Chagas disease patients [6] and patients with arrhythmogenic right ventricular cardiomyopathy [7].

However the main limitations of VLP analysis are an incomplete characterization of reentrant activity [8] and have a low positive predictive accuracy [4]. The reentrant activity excitation produced by the arrhythmic substrate is not always accompanied by VLP; it may be completely contained within the normal QRS period [9,10]. Gomis et al. [11] have proposed an autoregressive moving average (ARMA) model to quantify the abnormal intra-QRS potentials (AIQP), which are considered as low-amplitude notches and slurs with sudden changes in slope. Several studies have demonstrated that the estimated AIQP is a potential index for evaluating the risk of ventricular arrhythmias [11–14]. AIQP analysis has also been applied to noninvasively identify the mechanisms of premature ventricular beats [15] and to detect acute transmural myocardial ischemia [16].

However, it is not an easy job to accurately extract the AIQP when there is an extremely poor signal-noise-ratio (a low-amplitude AIQP compared with a large QRS wave). One of the main limitations of the ARMA modeling technique is that the true model order is unknown. A model order higher or lower than the true one would cause the estimated AIQP to be underestimated or involved with part of the normal QRS complex. The selected model order in the study of Gomis et al. [11] was dependent on clinical data. Although the cross correlation method [13] provides a basis for model order selection, it cannot confirm that the chosen model order is accurate. Another limitation is the estimation error of AIQP caused by the overlap between the normal QRS and the broad-band AIQP. The simulation results of our previous study [14] showed that the overlap between the normal QRS complex and AIQP in the low-frequency discrete cosine transform (DCT) coefficients caused a high estimation error, even when the selected model order was accurate. Furthermore, if the normal QRS complex also included dominant high-frequency components, especially caused by an abrupt *R* wave, the estimated AIQP would also include part of the normal QRS, and no model order can accurately separate AIQP.

Because of the difficulties in the extraction of AIQP, this study attempts to develop a new method to extract other useful signals within the QRS complex which can be applied to identify the ventricular tachycardia (VT) patients with high-risk ventricular arrhythmias. The basic idea of this study is to extend the detection

* Corresponding author at: No. 35, Lane 215, Sec. 1, Jhongshan Road, Taiping City, Taichung County 411, Taiwan. Tel.: +886 4 23924505x7238; fax: +886 4 23924419.
E-mail address: cclin@ncut.edu.tw

0010-4825/$ - see front matter © 2010 Elsevier Ltd. All rights reserved.
doi:10.1016/j.compbiomed.2010.05.002

of AIQP to all of the unpredictable components within the QRS complex which originate from the signals with sudden slope changes, including the sharp QRS wave and the transient AIQP. This study proposes a finite-impulse-response (FIR) prediction model to analyze the unpredictable intra-QRS potentials (UIQP). The FIR prediction technique has been widely applied in various studies; for example, QRS feature extraction [17], the enhancement of signal averaging in ventricular late potentials detection [18], the adaptive enhancement of multiple sinusoids in uncorrelated noise [19], the reduction of the interference in the secondary path modeling of active noise control systems [20], and so on. The aim of this study is to determine whether the UIQP detected by the prediction error of an FIR prediction model can be applied to diagnose patients with sustained VT and to improve the diagnostic performance of SAECG.

2. Methods

2.1. Data acquisition

This study followed the principles that (1) informed consent was obtained from each patient and (2) the Ethics Committee of Taipei Jen-Chi General Hospital had approved the study. The study subjects were divided into two groups, and were identical with our previous study [14]. Group I (normal group) comprised 42 normal Taiwanese (20 men and 22 women, aged 58 ± 14 years). Group II (VT group) consisted of 30 patients (15 men and 15 women, aged 63 ± 16 years). The VT patients were suffering from chronic ischemic heart disease after surviving clinically documented myocardial infarction (MI). The methods of recording high-resolution electrocardiograms have been described elsewhere [13]. The time unit was 0.5 ms per sample as a result of using a 2 kHz sampling rate. Three standardized time-domain SAECG parameters [4], namely filtered total QRS duration (fQRSD), RMS voltage of the last QRS 40 ms (RMS40) and duration of the low amplitude signals below 40 mV (LAS40), were performed to detect VLP.

2.2. Development of an FIR prediction model for estimating the unpredictable intra-QRS potentials

Fig. 1 is a block diagram of an FIR prediction model for estimating the UIQP, where D is the time-delay length or prediction depth and $W(z)$ denotes the z-transform system function of an FIR Wiener filter. The design of a Wiener filter is to produce the minimum mean-square estimate $\hat{d}(n)$ of a given desired input $d(n)$ by filtering a set of observations of a related reference input $x(n)$. The desired input $d(n)$ is the input QRS signal, and the input reference signal $x(n)$ is the delayed version of the input QRS, $x(n)=d(n-D)$; hence the FIR Wiener filter acts as a predictor that linearly combines the past values of the input QRS before D time units to predict the current value. The prediction

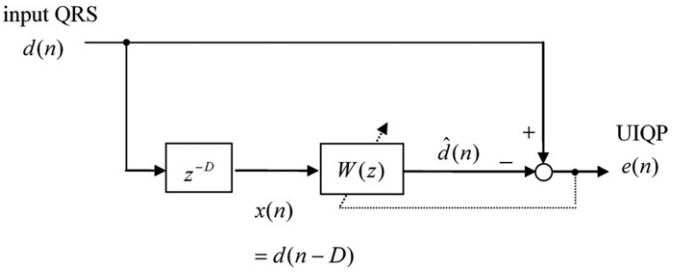

Fig. 1. Block diagram of an FIR prediction model for estimating the UIQP. FIR, finite-impulse-response; UIQP, unpredictable intra-QRS potentials.

output of the FIR filter with order $M-1$ has the form

$$\hat{d}(n) = x(n) \otimes w(n) = \sum_{i=0}^{M-1} w(i)x(n-i) \tag{1}$$

where $\otimes$ denotes the operation of convolution sum and $w(i)$ for $i=0, \ldots, M-1$ are the filter coefficients. The Wiener filter design problem needs to find the filter coefficients $w(i)$ that minimize the mean-square value of the prediction error $e(n)=d(n)-(n)$ defined as follows:

$$\xi = E\{|e(n)|^2\} = E\{|d(n)-\hat{d}(n)|^2\} \tag{2}$$

The necessary and sufficient condition for a set of filter coefficients to minimize ξ is that the derivative of ξ with respect to $w^*(k)$ must be equal to zero for $k=0, 1, \ldots, M-1$ (* denotes a complex conjugate operation). Assuming $x(n)$ and $d(n)$ are jointly wide sense stationary, then $E\{x(n-i)x^*(n-k)\}=r_x(k-i)$ and $E\{d(n)x^*(n-k)\}=r_{dx}(k)$ and the well-known Wiener-Hopf equations can be derived as follows [21]:

$$\sum_{i=0}^{M-1} w(i)r_x(k-i) = r_{dx}(k), \quad k = 0, 1, \ldots, M-1 \tag{3}$$

which is a set of M linear equations in the M unknowns $w(i)$, $i=0, 1, \ldots, M-1$.

The matrix form of the Wiener-Hopf equations can be written as

$$\begin{bmatrix} r_x(0) & r_x^*(1) & \cdots & r_x^*(M-1) \\ r_x(1) & r_x(0) & \cdots & r_x^*(M-2) \\ r_x(2) & r_x(1) & \cdots & r_x^*(M-3) \\ \vdots & \vdots & & \vdots \\ r_x(M-1) & r_x(M-2) & \cdots & r_x(0) \end{bmatrix} \begin{bmatrix} w(0) \\ w(1) \\ w(2) \\ \vdots \\ w(M-1) \end{bmatrix} = \begin{bmatrix} r_{dx}(0) \\ r_{dx}(1) \\ r_{dx}(2) \\ \vdots \\ r_{dx}(M-1) \end{bmatrix} \tag{4}$$

and

$$\mathbf{R}_x \mathbf{w}_o = \mathbf{r}_{dx} \tag{5}$$

where $\mathbf{R}_x$ is an $M \times M$ autocorrelation matrix of the reference input $x(n)$, $\mathbf{w}_o$ is an $M \times 1$ vector of the optimal filter coefficients, and $\mathbf{r}_{dx}$ is an $M \times 1$ vector of the cross-correlations between the desired input $d(n)$ and the reference input $x(n)$. This study introduces General Levinson Recursion [21] to recursively solve the Wiener-Hopf equations which are a set of Hermitian Toeplitz equations of the form given in Eq. (5).

The following section of simulation results demonstrates that the minimized prediction error $e(n)$ can be used to detect the slope changes at the slope discontinuities of the input QRS signal. To compare the prediction errors and the slope changes at the slope discontinuities, this study particularly defines a slope function as the amplitude changes per D time units,

$$s(n) = d(n)-d(n-D) \tag{6}$$

and a slope change function as the slope changes per D time units,

$$a(n) = s(n)-s(n-D) \tag{7}$$

2.3. Definition of UIQP parameters

This study introduces the prediction error of the FIR prediction model to analyze the UIQP for the diagnosis of VT patients. A root-mean-square (RMS) value of the prediction error within the entire QRS duration was defined to quantify the UIQP as follows:

$$\text{UIQP\_l}(D) = \sqrt{\frac{1}{\text{fQRSD}} \sum_{n=n_1}^{n_2} e^2(n)} \tag{8}$$

where l denotes lead X, Y or Z, D is the prediction depth, n_1 and n_2 are the onset and offset of the QRS complex, respectively, and $e(n)$ is the

prediction error. The study further defined a UIQP-to-QRS ratio (UQR) to normalize the UIQP by the RMS value of the QRS complex as follows:

$$\mathrm{UQR\_l} = \frac{\mathrm{UIQP\_l}}{\sqrt{\frac{1}{\mathrm{fQRSD}}\sum_{n=n_1}^{n_2} d^2(n)}} \tag{9}$$

where l denotes lead X, Y or Z, and $d(n)$ is the input QRS complex.

2.4. Classification of the normal and VT groups using Fisher's linear discriminant method

This study used Fisher's linear discriminant method [22] to combine the time-domain VLP and UIQP parameters and to classify the normal and VT groups. Assume $\mathbf{x}_1, \mathbf{x}_2, \ldots, \mathbf{x}_{N_1}$ are N_1 observations from VT patients and $\mathbf{x}_{N_1+1}, \mathbf{x}_{N_1+2}, \ldots, \mathbf{x}_{N_1+N_2}$ are N_2 observations from normal groups. Each observation $\mathbf{x}_i$, $i=1,2, \ldots, N_1+N_2$ is a $p\times 1$ vector consisting of UIQP and time-domain VLP parameters. The linear discriminant function is defined to transform each $p\times 1$ observation $\mathbf{x}_i$ to a single value g_i as follows:

$$g_i(\mathbf{x}_i) = \boldsymbol{\omega}^T\mathbf{x}_i, \quad i=1,2,\ldots,N_1+N_2 \tag{10}$$

where $\mathbf{x}_i$ denotes a $p\times 1$ vector; $\mathbf{x}_i^T = [x_{i1} \quad x_{i2} \quad \ldots \quad x_{ip}]$, $\boldsymbol{\omega}$ is a $p\times 1$ weight vector; $\boldsymbol{\omega}^T = [\omega_1 \quad \omega_2 \quad \ldots \quad \omega_p]$. The classical Fisher's discriminant method was applied to find the optimized weight vector which can maximize the separation function $|S(\boldsymbol{\omega})|$ defined as follows:

$$S(\boldsymbol{\omega}) = \frac{\overline{G}_1 - \overline{G}_2}{S_g} \tag{11}$$

where $\overline{G}_1$ and $\overline{G}_2$ are the mean values of the transformed observations of VT and normal groups, respectively; $\overline{G}_1 = (1/n_1)\sum_{i=1}^{N_1} g_i$ and $\overline{G}_2 = (1/N_2)\sum_{i=N_1+1}^{N_1+N_2} g_i$, and S_g is the standard deviation of the transform observations defined as follows:

$$S_g = \sqrt{\frac{\sum_{i=1}^{N_1}(g_i - \overrightarrow{G_1})^2 + \sum_{i=N_1+1}^{N_1+N_2}(g_i - \overline{G}_2)^2}{N_1+N_2-2}} \tag{12}$$

The separation function measures the difference between the transformed means $\overline{G}_1 - \overline{G}_2$ expressed in standard deviation units. The optimized weight vector can be found by solving the first derivative of the separation function $(\partial S(\boldsymbol{\omega})/\boldsymbol{\omega} = 0)$ and can be further simplified as follows:

$$\hat{\boldsymbol{\omega}} = \mathbf{S}_{\mathrm{pooled}}^{-1}(\overline{\mathbf{X}}_1 - \overline{\mathbf{X}}_2) \tag{13}$$

where $\overline{\mathbf{X}}_1$ and $\overline{\mathbf{X}}_2$ are the mean vectors of the observations from the VT and normal groups, respectively; $\overline{\mathbf{X}}_1 = (1/N_1)\sum_{i=1}^{N_1}\mathbf{x}_i$ and $\overline{\mathbf{X}}_2 = 1/N_2\sum_{i=N_1+1}^{N_1+N_2}\mathbf{x}_i$, and the matrix $\mathbf{S}_{\mathrm{pooled}}$ is the weighted average of the sample covariance matrices $\mathbf{S}_1$ and $\mathbf{S}_2$ of the VT and normal groups given by

$$\mathbf{S}_{\mathrm{pooled}} = \frac{(N_1-1)\mathbf{S}_1 + (N_2-1)\mathbf{S}_2}{N_1+N_2-2} \tag{14}$$

where $\mathbf{S}_1 = \frac{\sum_{i=1}^{N_1}(\mathbf{x}_i-\overline{\mathbf{X}}_1)(\mathbf{x}_i-\overline{\mathbf{X}}_1)^T}{N_1-1}$ and $\mathbf{S}_2 = \frac{\sum_{i=N_1+1}^{N_1+N_2}(\mathbf{x}_i-\overline{\mathbf{X}}_2)(\mathbf{x}_i-\overline{\mathbf{X}}_2)^T}{N_1-1}$.

The critical value with minimum expected cost of misclassification for separating the VT and normal groups can be derived as follows [22]:

$$\hat{m} = \frac{\overline{G}_1 + \overline{G}_2}{2} \tag{15}$$

Three clinical performance indices including specificity (SP), sensitivity (SE) and total prediction accuracy (TPA) [23] were then calculated to evaluate the local performance of the diagnosis of the VT patients from the normal subjects.

3. Results

3.1. Simulation studies of the FIR prediction modeling technique

The first simulation study adopted a positive triangular wave (900 μV peak value, 90 ms duration) to simulate a sharp R wave, and a low-amplitude, transient positive triangular wave (30 μV peak value, 2.5 ms duration, located at 130 ms) to simulate the AIQP. The slopes m_1 and m_2 (μV/ms) of straight lines L_1 and L_2 were 30 and −15, respectively. Fig. 2(a) also shows the prediction output (dotted line) using a second-order FIR prediction model with a prediction depth D of 4 (2 ms). The prediction errors can be found at the slope discontinuities of time 70, 100, 130 and 160 ms, respectively. Fig. 2(b) particularly shows the prediction results around time 100 ms. The main prediction errors starting from the time 100 ms were close to −22.5, −45, −67.5 and −90 μV. From the simulation results it can be observed that there were D data points exhibiting obvious prediction errors at each slope discontinuity, and the prediction error at the Dth data point was close to $(D/2)\times(m_2-m_1)$ if the slope was suddenly changed from m_1 to m_2. Fig. 2(c) plots the slope function defined in Eq. (6). Fig. 2(d) further compares the slope changes (solid line) defined in Eq. (7) and the prediction error (dashed line). It can be found that the prediction error can be applied to detect the slope changes at the slope discontinuities, if the prediction output can accurately estimate the smoothed part of the input signal. It is also worth noting that the low-amplitude, transient triangular wave also induced a large slope change because of its sudden change in slope.

The second simulation study used an X lead QRS complex from the normal group to simulate the normal QRS complex, and a normally distributed white noise with zero mean and RMS value of 5 μV to simulate the low-amplitude AIQP, as shown in Fig. 3(a). The display of the white noise was enlarged 5 times to clearly show the waveform of the simulated AIQP. Fig. 3(b) compares the UIQPs of the normal QRS complex adding (dashed line) and not adding (solid line) AIQP. The UIQP was detected by the prediction error of a 10th-order FIR prediction model with the prediction depth $D=4$. Both the RMS values of the normal QRS complex with and without AIQP were adjusted to be equal to 500 μV. The QRS complex adding AIQP showed a higher RMS value of UIQP in comparison with one not adding AIQP, 23.4 μV vs. 17.5 μV, respectively. However, if the RMS value of the normal QRS complex was amplified 2 times to 1000 μV; that of the UIQP was proportionally increased to 35.0 μV because of the linearity of the FIR prediction model. To reduce the effect of the magnitude of the QRS complex, this study defined the UQR parameter to normalize the UIQP parameter by the RMS value of the QRS complex. Both the UQRs of the normal QRS complex with RMS values of 500 μV and 1000 μV were 3.5%, which is lower than the 4.68% of the QRS complex including AIQP.

3.2. Clinical results

The model order and the prediction depth are the critical parameters of the FIR prediction modeling technique. This study performed the UIQP analyses using various model orders and prediction depths to determine the most suitable of each. Fig. 4(a–c), show the curves of mean UQR vs. the model order for the normal and VT groups in leads X, Y and Z, respectively. The prediction depth D was fixed at 4. The decreases of the mean UQR both in the normal and VT groups are very small, and the difference between the normal and the VT groups does not change significantly when the order is higher than 10. This is because the signals with sudden slope changes cannot be predicted, even if an order higher than the sufficient one is used. Hence a model order of 10 is sufficient for the analysis of UIQP.

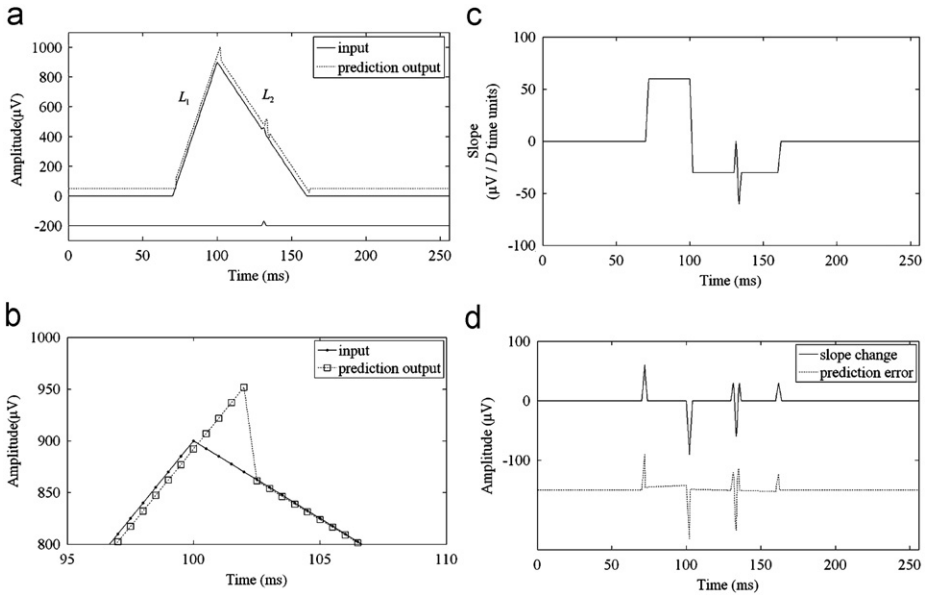

Fig. 2. Prediction results of a second-order FIR prediction model with a prediction depth of $D=4$ for the input of a large positive triangular wave adding a low-amplitude, transient triangular wave located at time 130 ms: (a) the prediction output (dotted line) and the input triangular wave (solid line); (b) the prediction output (dotted line with squares) and the input triangular wave (solid line with points) around time 100 ms; (c) the slope function of the input signal; and (d) the slope changes at slope discontinuities (solid line), and the prediction error (dotted line). 1 time unit = 0.5 ms.

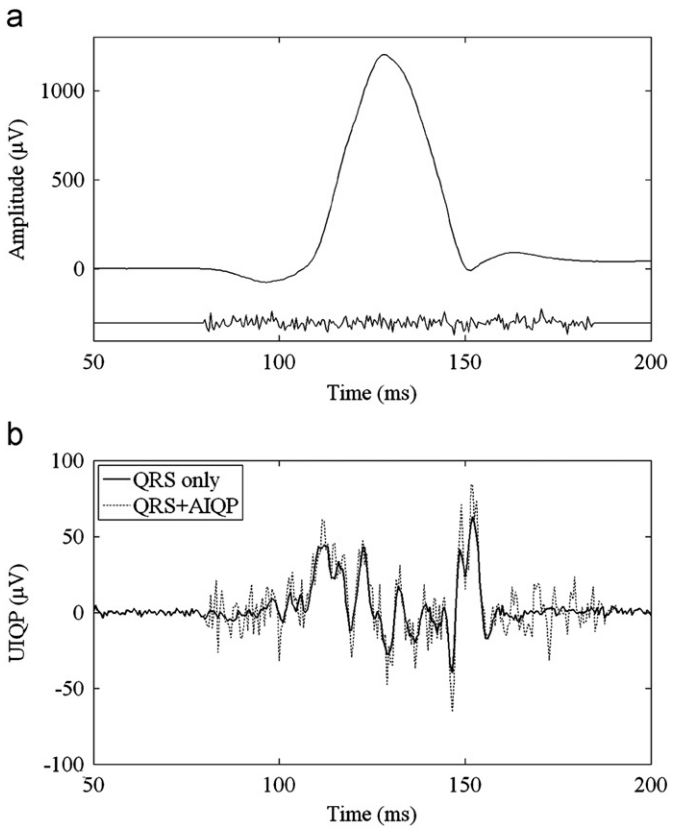

Fig. 3. Comparisons of the UIQPs of a normal QRS complex adding and not adding the simulated AIQP: (a) an X lead QRS complex of a normal subject simulating the normal QRS complex and a normally distributed white noise with zero mean simulating the AIQP; (b) the detected UIQPs of the QRS complex with (dashed line) and without (solid line) AIQP using a 10th-order FIR prediction model with the prediction depth $D=4$.

Fig. 5(a) plots the curves of TPA vs. the prediction depth using a 10th-order FIR prediction model in leads *X*, *Y* and *Z*, respectively. A medium prediction depth of 4 has the maximum mean value 75.0% of TPA of leads *X*, *Y* and *Z*. Fig. 5(b) further plots the curves of mean signal-to-noise ratio (SNR) vs. the prediction depth, including all study subjects in leads *X*, *Y* and *Z*. A 40 ms segment in which the RMS value of the prediction error was the minimum in the ST segment was defined to evaluate the background noise level. The SNR was then defined as the ratio between the UIQP and background noise level. It can be found that a larger prediction depth can increase the SNR.

Table 1 lists the results of the UIQP and time-domain VLP parameters, where the UIQP parameters in leads *X*, *Y* and *Z* were detected using a 10th-order FIR prediction model with the prediction depth $D=4$. The results of the time-domain VLP parameters are consistent with previous studies [15,16]. Both the mean RMS values of the UIQP and the QRS complex of the VT patients in leads *Y* and *Z* were significantly lower than those of the normal subjects ($p<0.05$). The mean UQRs of the VT patients in leads *X*, *Y* and *Z* were all significantly higher than those of the normal subjects ($p<0.05$).

Table 2 demonstrates the clinical performance of UQR and time-domain VLP parameters for the diagnosis of the VT patients. The best TPA using individual UQR parameters was 79.2% of UQR_X, which is superior to 68.1% of fQRSD, 75.0% of RMS40 and 70.8 of LAS40. The linear combination of UQR parameters of leads *X*, *Y* and *Z* gives a small increase in TPA to 80.6%. The linear combination of UQR and time-domain VLP parameters can further increase the TPA to 84.7% (specificity 81.0% and sensitivity 90.0%). The logical combination of any 2 of the UQR parameters also gives an increase in TPA to 83.3%. The logical combination of any 4 of the UQR and time-domain VLP parameters can further increase the TPA to 87.5% (specificity 88.1% and sensitivity 86.7%)

4. Discussion

4.1. Technical aspects of the FIR prediction modeling technique for detecting the unpredictable intra-QRS potentials

This study has presented the FIR prediction modeling technique to detect the UIQP for the diagnosis of VT patients with high-risk ventricular arrhythmias instead of the extraction of the AIQP.

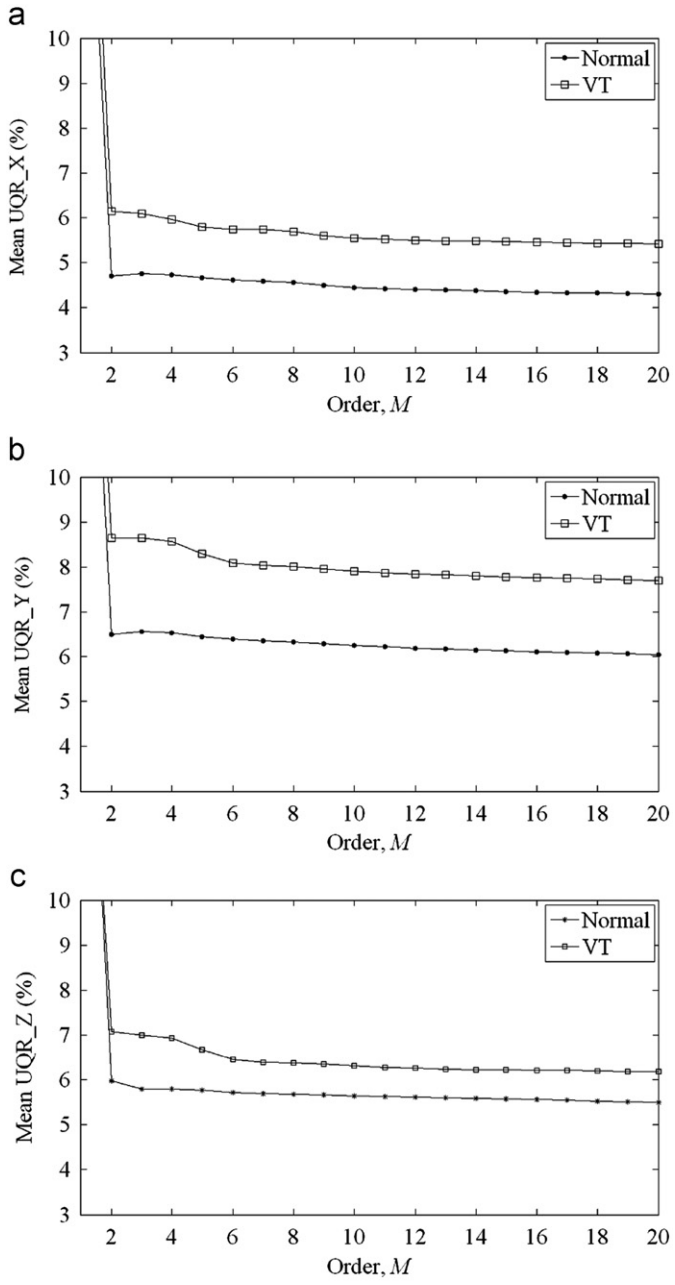

Fig. 4. Curves of mean UQR vs. the model order in leads (a) *X*, (b) and (c) *Z*. The prediction depth *D* was fixed at 4.

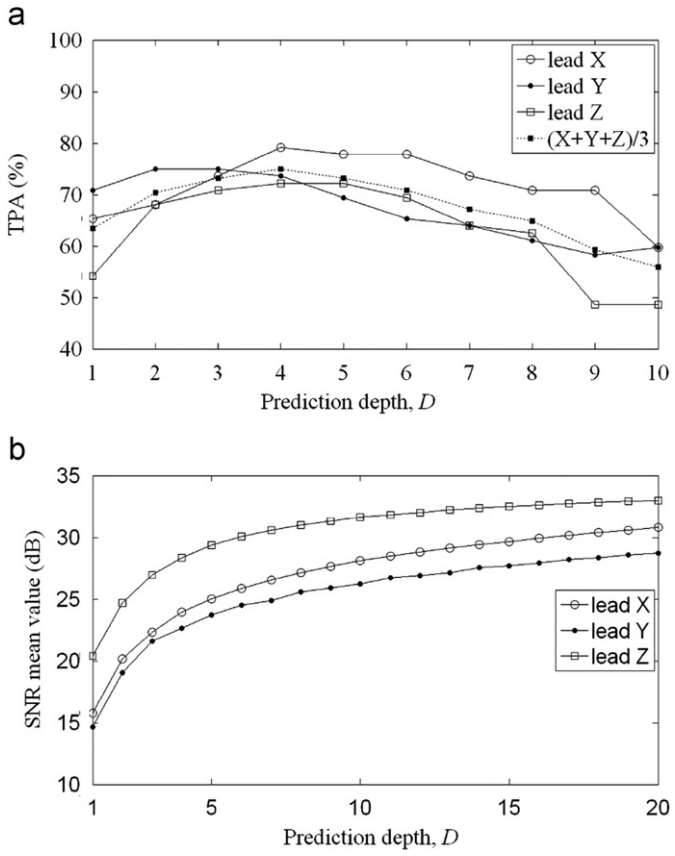

Fig. 5. Curves of (a) TPA and (b) SNR mean value vs. the prediction depth using a 10th-order FIR prediction model.

Table 1
UIQP and time-domain VLP parameters for the normal and VT groups.

	Normal	VT
Time domain VLP parameters		
fQRSD (ms)	90.3 ± 10.2	$96.5 \pm 7.7^{**}$
RMS40 (μV)	43.7 ± 25.0	$20.1 \pm 9.6^{**}$
LAS40 (ms)	29.0 ± 5.7	$37.2 \pm 6.7^{**}$
UIQP parameters		
UIQP_X (μV)	23.4 ± 6.6	24.0 ± 9.9^{NS}
UIQP_Y (μV)	37.2 ± 11.5	$28.9 \pm 12.1^{**}$
UIQP_Z (μV)	37.8 ± 14.5	$31.9 \pm 10.6^{*}$
RMS values of the QRS complex		
QRS_X (μV)	537.7 ± 170.4	513.2 ± 299.9^{NS}
QRS_Y (μV)	625.6 ± 236.5	$432.0 \pm 239.8^{**}$
QRS_Z (μV)	677.8 ± 245.2	$540.5 \pm 253.4^{*}$
UIQP-to-QRS ratios		
UQR_X (%)	4.4 ± 0.7	$5.5 \pm 1.9^{**}$
UQR_Y (%)	6.3 ± 1.3	$7.9 \pm 3.4^{**}$
UQR_Z (%)	5.6 ± 1.1	$6.3 \pm 1.4^{*}$

The UIQP of leads *X*, *Y* and *Z* were detected using a 10th-order FIR prediction model with a prediction depth $D=4$.UIQP_l, QRS_l and UQR_l are the unpredictable intra-QRS potentials, root-mean-square value of QRS complex, and UIQP to QRS ratio in lead *l*, where $l=X, Y, Z$, respectively.Student's two-tailed *t*-test was performed to compare the means of the two independent variables.

^{NS} Non-significant ($p > 0.05$); compared to the normal group.
* $p < 0.05$; compared to the normal group.
** $p < 0.01$ compared to the normal group.

The UIQP originates from the signals with sudden slope changes within the QRS complex, including the sharp QRS wave and the AIQP. The simulation study has shown that the UIQP can be detected as the slope changes at slope discontinuities by the prediction error, and a QRS complex with AIQP has a larger UIQP in comparison with one without AIQP. The UIQP is not only dominated by the sharpness of the QRS wave and the AIQP, but also by the magnitude of the QRS wave because of the linearity of the FIR prediction model. Hence a UIQP-to-QRS ratio was further defined to normalize the UIQP parameters by the RMS value of the QRS complex.

The determinations of the model order and prediction depth are critical in the FIR prediction modeling technique. The model order must be sufficient to accurately predict the smoothed part of the input QRS complex. The clinical results show that the use of a model order higher than the sufficient one only slightly increased the prediction accuracy of the smoothed part of the QRS complex because the signals with sudden changes in slope cannot be predicted. It cannot increase the difference of the mean

Table 2
Clinical performance of UQR and time-domain VLP parameters.

	SP (%)	SE (%)	TPA (%)
Time-domain VLP parameters			
fQRSD	64.3	73.3	68.1
RMS40	64.3	90.0	75.0
LAS40	71.4	70.0	70.8
UIQP-to-QRS ratios			
UQR_X	78.6	80.0	79.2
UQR_Y	73.8	73.3	73.6
UQR_Z	71.4	73.3	72.2
Linear combination			
$-0.04 \times \text{RMS40} + 0.14 \times \text{LAS40}$	73.8	73.3	73.6
$0.57 \times \text{UQR\_X} + 0.16 \times \text{UQR\_Y} + 0.63 \times \text{UQR\_Z}$	81.0	80.0	80.6
$0.49 \times \text{UQR\_X} + 0.09 \times \text{UQR\_Y} + 0.76 \times \text{UQR\_Y} - 0.0002 \times \text{fQRSD} - 0.04 \times \text{RMS40} + 0.12 \times \text{LAS40}$	81.0	90.0	84.7
Logical combination			
Any 2 of time-domain VLP parameters	64.3	76.7	69.4
Any 2 of UQR parameters	85.7	80.0	83.3
Any 3 of UQR and time-domain VLP parameters	81.0	93.3	86.1
Any 4 of UQR and time-domain VLP parameters	88.1	86.7	87.5

UQR parameters between the normal and VT groups. The clinical results suggest that a model order of 10 is sufficient for the analysis of UIQP. In addition, the study results show that a medium prediction depth of 4 has the best diagnosis performance for VT patients. It is possible that too small or too large a prediction depth will decrease the clinical performance because a smaller prediction depth can reduce the SNR (UIQP vs. background noise level) as shown in Fig. 5(b), and a, larger prediction depth can produce larger prediction errors and more error points at each slope discontinuity.

4.2. Clinical results of the UIQP analysis

Because of their abnormal myocardial conduction, the VT patients were expected to display increased UIQP. On the contrary, the study results show that the mean UIQPs in leads *Y* and *Z* were significantly decreased in VT patients. This is possibly caused by the effects of the magnitude of the QRS complex. The simulation study shows that the UIQP is proportional to the RMS value of the input QRS complex if the input QRS complexes have the same shape because of the linearity of the FIR prediction model. The clinical results further demonstrate that the RMS values of the QRS complex in leads *Y* and *Z* were also significantly decreased in VT patients, and the RMS values of the QRS complex in the normal and VT groups both had a wide range from 200 to 1400 μV. The reduced RMS values of the QRS complex and the UIQP in VT patients may be related with MI. Bhargava and Goldberger [24] and Talwar et al. [25] have shown that MI attenuates both low and high frequency QRS potentials. From a pathophysiological viewpoint, myocardial necrosis leads to a general decrease in electromotive potentials.

In view of the above, it cannot be determined that a larger UIQP is produced by a larger magnitude of the QRS complex or from the AIQP, even if the sharpness of the QRS complex is similar. Hence the UIQP-to-QRS ratio is proposed in this study to reduce the effects of the magnitude of the QRS complex. The clinical results demonstrate that the mean UIQP-to-QRS ratios of VT patients were significantly larger than those of the normal group in leads *X*, *Y* and *Z* ($p < 0.05$). Both the linear and logical combinations of the UIQP-to-QRS ratios and time-domain VLP parameters can further enhance the diagnosis performance for VT patients.

4.3. Comparisons between the analyses of UIQP and AIQP

The AIQP analysis [11–14] is concentrated on the extraction of the low-amplitude, transient signals within the entire QRS complex. However the extremely low SNR (AIQP vs. QRS complex) and the overlap between the AIQP and QRS complex in the time and frequency domains limits the accuracy of the AIQP extraction using the ARMA model in the discrete transform domain. The UIQP analysis proposed in this study is focused on the detection of all the signals with sudden slope changes, possibly including the sharp QRS wave and the transient AIQP. The study results show that the UIQP can be detected as the slope changes at the slope discontinuities by the prediction error of an FIR prediction model.

The significant reductions of UIQP in VT patients is consistent with our previous studies using the ARMA modeling technique to extract AIQP [13,14]. One previous study [13] has shown that a higher risk of ventricular arrhythmias was associated with lower AIQP in lead *Y*. The other study [14] recruiting the same subjects as used in this study also showed that the mean high-frequency AIQP parameters of VT patients were significantly lower than those of the healthy group in leads *Y* and *Z*. However the significant reductions of AIQP in VT patients may also be related with the reductions of the RMS values of the QRS complex. Because the extracted AIQP is also proportional to the magnitude of the QRS complex due to the linearity of the ARMA model, this study suggests that the AIQP analysis can further consider normalizing the AIQP parameter by the RMS value of the QRS complex.

5. Conclusions

This study has successfully demonstrated that the UIQP, originating from the signals with sudden slope changes, can be detected as the slope changes at the slope discontinuities, using the FIR prediction modeling technique. The clinical results also demonstrate that the VT patients had a larger UIQP-to-QRS ratio in comparison with the normal subjects, and the linear and logical combinations of UIQP-to-QRS ratios and time-domain VLP parameters can increase the diagnosis performance of SAECG. Hence the UIQP-to-QRS ratio analyzed using the FIR prediction modeling technique may be a new promising index for the diagnosis of VT patients.

6. Summary

The abnormal intra-QRS potentials (AIQP) have been proposed as a risk evaluation index for ventricular arrhythmias. However it is difficult to accurately extract the low-amplitude AIQP because of the extremely low signal-to-noise ratio (AIQP vs. the QRS complex) and the overlap between AIQP and the QRS complex. This study proposes the analysis of unpredictable intra-QRS potentials (UIQP) using a finite-impulse-response (FIR) prediction model for the diagnosis of ventricular tachycardia (VT) patients with high-risk ventricular arrhythmias, instead of the extraction of the AIQP. The UIQP originates from the signals with sudden slope changes within the QRS complex, including the sharp QRS complex and the AIQP. Using the prediction error of the proposed FIR prediction model, the UIQP can be detected as the slope changes at slope discontinuities within the QRS complex. The study subjects were composed of 42 normal Taiwanese and 30 VT patients. The simulation study demonstrates that the presence of the AIQP can increase the UIQP. Because the UIQP is proportional to the magnitude of the QRS complex due to the linearity of the FIR prediction model, this study defines a UIQP-to-noise ratio (UQR) to normalize the UIQP by the root-mean-square value of the QRS complex. The clinical results show that the mean UQRs of the VT patients in leads *X*, *Y* and *Z* are significantly higher than those of the normal subjects, and the linear and logical combinations of UQR and time-domain ventricular late potentials parameters can increase the diagnosis performance to a total predictive accuracy of 84.7% (specificity 81.0% and sensitivity 90.0%) and 87.5% (specificity 88.1% and sensitivity 86.7%), respectively.

Conflict of interest statement

None declared.

Acknowledgments

The author would like to thank the National Science Council of the Republic of China, Taiwan, for financially supporting this research under Contract no. 97-2320-B-167-001. Staff of the Hemodialysis Unit and patients of the Cardiology Department at Jen-Chi General Hospital are appreciated for their kind assistance and cooperation in this investigation.

References

[1] M.B. Simson, Use of signals in the terminal QRS complex to identify patients with ventricular tachycardia after myocardial infarction, Circulation 64 (1981) 235–242.
[2] J.R. Jarrett, N.C. Flowers, Signal-averaged electrocardiography: history, techniques, and clinical applications, Clinical Cardiology 14 (1991) 984–994.
[3] G. Breithardt, M.E. Cain, N. El-Sherif, N. Flowers, V. Hombach, M. Janse, M.B. Simson, G. Steinbeck, Standards for analysis of ventricular late potentials using high-resolution or signal-averaged electrocardiography: a statement by a task force committee of the European Society of Cardiology, the American Heart Association, and the American College of Cardiology, Journal of the American College of Cardiology 17 (1991) 999–1006.
[4] M.E. Cain, J.L. Anderson, M.F. Arnsdorf, J.W. Mason, M.M. Scheinman, A.L. Waldo, Signal-averaged electrocardiography, Journal of the American College of Cardiology 27 (1996) 238–249.
[5] H. Tatsumi, M. Takagi, E. Nakagawa, H. Yamashita, M. Yoshiyama, Risk stratification in patients with Brugada syndrome: analysis of daily fluctuations in 12-lead electrocardiogram (ECG) and signal-averaged electrocardiogram (SAECG), Journal of Cardiovascular Electrophysiology 17 (2006) 705–711.
[6] A.L. Ribeiro, P.S. Cavalvanti, F. Lombardi, M.C. Nunes, M.V. Barros, M.C. Rocha, Prognostic value of signal-averaged electrocardiogram in Chagas disease, Journal of Cardiovascular Electrophysiology 19 (2008) 502–509.
[7] A.F. Folino, B. Bauce, G. Frigo, A. Nava, Long-term follow-up of the signal-averaged ECG in arrhythmogenic right ventricular cardiomyopathy: correlation with arrhythmic events and echocardiographic findings, Europace 8 (2006) 423–429.
[8] P. Lander, E.J. Berbari, C.V. Rajagopalan, P. Vatterott, R. Lazzara, Critical analysis of the signal-averaged electrocardiogram. Improved identification of late potentials, Circulation 87 (1993) 105–117.
[9] H.J. Schwarzmaier, U. Karbenn, M. Borggrefe, J. Ostermeyer, G. Breithardt, Relation between ventricular late endocardial activity during intraoperative endocardial mapping and low amplitude signals within the terminal QRS complex on the signal-averaged surface electrocardiogram, The American Journal of Cardiology 66 (1990) 308–314.
[10] P.T. Vaitkus, K.E. Kindwall, F.E. Marchlinski, J.M. Miller, A.E. Buxton, M.E. Josephson, Differences in electrophysiological substrate in patients with coronary artery disease and cardiac arrest or ventricular tachycardia. Insights from endocardial mapping and signal-averaged electrocardiography, Circulation 84 (1991) 672–678.
[11] P. Gomis, D.L. Jones, P. Caminal, E.J. Berbari, P. Lander, Analysis of abnormal signals within the QRS complex of the high-resolution electrocardiogram, IEEE Transactions on Biomedical Engineering 44 (1997) 681–693.
[12] P. Lander, P. Gomis, R. Goyal, E.J. Berbari, P. Caminal, R. Lazzara, J.S. Steinberg, Analysis of abnormal intra-QRS potentials. Improved predictive value for arrhythmic events with the signal-averaged electrocardiogram, Circulation 95 (1997) 1386–1393.
[13] C.C. Lin, C.M. Chen, I.F. Yang, T.F. Yang, Automatic optimal order selection of parametric modeling for the evaluation of abnormal intra-QRS signals in signal-averaged electrocardiograms, Medical and Biological Engineering and Computing 43 (2005) 218–224.
[14] C.C. Lin, Enhancement of accuracy and reproducibility of parametric modeling for estimating abnormal intra-QRS potentials in signal-averaged electrocardiograms, Medical Engineering and Physics 30 (2008) 834–842.
[15] E.J. Berbari, E.A. Bock, A.C. Chazaro, X. Sun, L. Sornmo, High-resolution analysis of ambulatory electrocardiograms to detect possible mechanisms of premature ventricular beats, IEEE Transactions on Biomedical Engineering 52 (2005) 593–598.
[16] P. Lander, P. Gomis, S. Warren, G. Hartman, K. Shuping, R. Lazzara, G. Wagner, Abnormal intra-QRS potentials associated with percutaneous transluminal coronary angiography-induced transient myocardial ischemia, Journal of Electrocardiology 39 (2006) 282–289.
[17] K.P. Lin, W.H. Chang, QRS feature extraction using linear prediction, IEEE Transactions on Biomedical Engineering 36 (1989) 1050–1055.
[18] A. Taboada-Crispi, J.V. Lorenzo-Ginori, D.F. Lovely, Adaptive line enhancing plus modified signal averaging for ventricular late potential detection, Electronics Letters 35 (1999) 1293–1295.
[19] J. Zeidler, E. Satorius, D. Chabries, H. Wexler, Adaptive enhancement of multiple sinusoids in uncorrelated noise, IEEE Transactions on Speech and Audio Processing ASSAP 26 (1978) 240–254.
[20] S.M. Kuo, D. Vijayan, A secondary path modeling technique for active noise control systems, IEEE Transactions on Speech and Audio Processing 5 (1996) 374–377.
[21] M.H. Hayes, Statistical Digital Signal Processing and Modeling, p. 268, p. 338, John Wiley & Sons Inc, 1996.
[22] R.A. Johnson, D.W. Wichern, Applied Multivariate Statistical Analysis, p. 581, Prentice-Hall Inc, 2002.
[23] P.F. Griner, R.J. Mayewski, A.I. Mushlin, P. Greenland, Selection and interpretation of diagnostic tests and procedures. Principles and applications, Annals of Internal Medicine 94 (1981) 557–592.
[24] V. Bhargava, A. Goldberger, Myocardial infarction diminishes both low and high frequency QRS potentials: power spectrum analysis of lead II, Journal of Electrocardiology 14 (1) (1981) 57–60.
[25] K.K. Talwar, G.S. Rao, U. Nayar, M.L. Bhatia, Clinical significance of high frequency QRS potentials in myocardial infarction: analysis based on power spectrum of lead III, Cardiovascular Research 23 (1) (1989) 60–63.

Chun-Cheng Lin is an Assistant Professor in Department of Electrical Engineering at National Chin-Yi University of Technology, Taiwan. He received his B.S. (1996), M.S. (1998) and Ph.D. degrees (2005) in Department of Electrical Engineering from National Taiwan University of Science and Technology, Taipei, Taiwan, respectively. His major research interests include computerized electrocardiogram analysis, biomedical signal processing and modeling, and active noise control.